Chemistry & Biology, Vol. 11, 121–126, January, 2004, ©2004 Elsevier Science Ltd. All rights reserved. DOI 10.1016/j.chembiol.2003.12.013

Conversion of Squalene to the Pentacarbocyclic Hopene

Dirk J. Reinert,[1] Gianni Balliano,[2] and Georg E. Schulz[1,*]
[1]Institut für Organische Chemie und Biochemie
Albert-Ludwigs-Universität, Albertstr. 21
D-79104 Freiburg
Germany
[2]Dipartimento di Scienza e Tecnologia del Farmaco
Via P. Giuria 9
I-10125 Torino
Italy

Summary

The membrane protein squalene-hopene cyclase was cocrystallized with 2-azasqualene and analyzed by X-ray diffraction to 2.13 Å resolution. The conformation of this close analog was clearly established, and it agreed with the common textbook presentation. The bound squalene undergoes only small conformational changes during the formation of rings A through D, thus requiring no intermediate. However, ring E formation is hindered by an entropic barrier, which may explain its absence in the steroids. The structure analysis revealed a mobile region between the active center cavity and the membrane, which may melt, opening a passage for squalene and hopene.

Introduction

The enzyme-catalyzed cyclization of terpenes via carbocationic transition states gives rise to numerous natural products, more than 25,000 of which have been established to this day [1]. The resulting terpenoids depend critically on the active center geometry of the respective enzyme. Some of the enzyme structures are presently known [2–7], and a structural support for the reaction sequence was obtained for a sesquiterpene [3] and for a monoterpene [7]. In particular, the cyclization of the triterpenes squalene and 2,3-oxidosqualene into various polycarbocyclic compounds, including hopene (bacteria), lanosterol (vertebrates and fungi), and cycloartenol (plants) has thrilled chemists for half a century [8–10]. The only structurally known enzyme of this group is the squalene-hopene cyclase (SHC) from *Alicyclobacillus acidocaldarius*, which is a homodimeric monotopic membrane protein [2, 11]. Its active center is located in a large elongated cavity (Figure 1). Squalene uptake and hopene release occur through a nonpolar channel connecting the active center cavity to the membrane-immersed region of the enzyme and thus to the membrane interior [12]. The top of the cavity contains Asp376, which donates the initial proton to the 2-3 double bond of squalene, creating a carbocation at C2 [2, 13]. The reaction proceeds through further carbocations until the final hopenyl cation is quenched via deprotonation by a water molecule [11]. Here, we report the high-resolution structure of the inhibitor 2-azasqualene [14] as bound to SHC and deduce from it the geometry and pathway of the cyclization reaction.

*Correspondence: schulz@bio.chemie.uni-freiburg.de

Results and Discussion

High quality data of a cocrystal were collected at 100 K, and the structure was solved by difference-Fourier techniques based on the well-established model of the SHC polypeptide [15]. The refinement at 2.13 Å resolution resulted in an R_{cryst} (R_{free}) value of 18.6% (22.8%) at good geometry. The initial (F_o-F_c)-density map calculated after a rigid body refinement already outlined the bound 2-azasqualene in detail in all three crystallographically independent subunits. The tertiary amine of the analog forms a salt bridge to Asp376 at the top of the active center cavity, and its last isoprene unit contacts Phe434 at the bottom (Figure 2). The limited length and the shape of the cavity enforce the observed meandering conformation, which corresponds to the common expectation illustrated in numerous textbooks (Figure 1A). About a dozen interactions between CH groups and π-electrons of triterpene double bonds as well as of aromatic residues [16, 17] can be discerned, but their influence on the conformation appears to be small.

Because of its close similarity to the bound inhibitor, the initial conformation of squalene was taken as that of 2-azasqualene except for the exchange of the nitrogen to an isoprenoid carbon. A molecular dynamics run changed the squalene conformation only slightly (Figure 3A). As observed with other inhibitors carrying a tertiary amine [15, 18], 2-azasqualene forms a salt bridge to Asp376, displacing it from its native position. Therefore, we added the Asp376 of an inhibitor-free SHC structure (refined at 2.1 Å resolution to an R_{cryst}/R_{free} value of 20%/24%; data not shown), which is optimally located and oriented to protonate the 2-3 double bond of squalene (3.3 Å distance to the C3 atom), generating the initial tertiary carbocation at C2. The reprotonation of Asp376 is achieved by a line of three hydrogen bonds connecting it to the bulk solvent and thus to the cytosol (Figure 3A).

The first five isoprene units of squalene meander in such a way that the formation of rings A through D requires only small displacements. The distances from the initial tertiary cation at C2 to the double-bonded C7 and from the second tertiary cation at C6 to the double-bonded C11 are about 4 Å each (Figure 3A). Moreover, the π-orbitals point to the respective cations, so that a low-barrier Markovnikov-type cation-olefin addition can be expected. This results in the 6-membered rings A and B in chair conformation and places a third tertiary cation at C10. The geometry is well set to add the C10 cation to the 14-15 double bond. This addition should result in a 5-membered ring C, which is favored entropically and by an energy difference of 50 kJ/mol [19] between the tertiary cation at C15 compared to a secondary cation at C14 that would emerge from an anti-

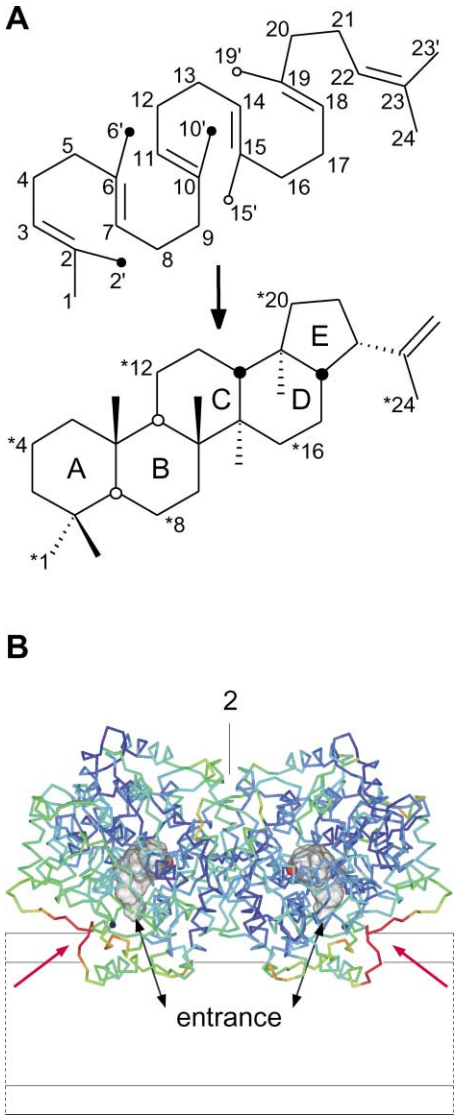

Figure 1. Reaction and Enzyme

(A) Squalene (top, IUPAC numbering) shown in the required conformation for cyclization to hopene. As indicated by stars, the hopene numbers refer to squalene. The inhibitor 2-azasqualene contains a nitrogen at position 2 and no 2-3 double bond. During the reaction, the methyl groups go above (filled circles) or below (open circles) the paper plane. Hopene hydrogens above (filled circles) and below (open circles) the paper plane define four of the nine chiral centers. Rings A to D assume chair conformations. In contrast to hopene, the steroid scaffold contains ring B in a boat conformation because the C10′ atom goes down during cyclization.

(B) Mobility plot of subunits A and B of dimeric squalene-hopene cyclase immersed in the membrane. The Cα atoms are color coded from blue (20 Å^2) to red (38 Å^2) for the TLS-corrected B factors [30]. Educt and product pass through a channel (black arrow) between the active center cavity (Asp376 marked as red dot) and the membrane interior. The outer channel wall including Phe434 (black dot) is mobile (red arrows) and therefore likely to open up, facilitating the passage.

Markovnikov closure to a 6-membered ring. However, since a cation at C14 is properly positioned to add to the 18-19 double bond (Figure 3A), it is more likely that a 6-membered ring C is formed in concert with a Markovnikov-type 5-membered ring D, generating a cation at C19 [19–21]. The resulting 6-6-6-5 tetracycle has the correct chair-chair-chair conformation of hopene.

Before the cyclization cascade can continue, the 22-23 double bond of the last isoprene unit has to approach the C19 cation. This involves a movement from the right side of Figure 3B to the left side. No such displacement was observed in any of the molecular dynamics runs using the 6-6-6-5 tetracycle. A closer inspection showed that this movement is possible but that it requires the coordinated rotations of several bonds, indicating an entropic barrier that was obviously too high to be overcome in molecular dynamics runs. From the observed geometry we therefore conclude that the cascade pauses at the 6-6-6-5 cation. This agrees with the observation of 6-6-6-5 compounds as by-products of wild-type SHC and as major products of various mutants [22, 23]. As soon as the 22-23 double bond reaches the tertiary cation at C19, it also stabilizes an intermediate secondary cation at C18 so that a concerted D-ring expansion with Markovnikov-type E ring formation can take place and generate the hopenyl cation at C23.

The hopenyl cation is then quenched by the putative water molecule X (Figure 3B) that either deprotonates C23′ or adds to C23 as a hydroxyl. Water X has never been observed in any SHC structure, indicating that it has no defined binding site. However, after the hopenyl cation has been formed, there is enough space in the cavity to accommodate water X with a hydrogen bond to water molecule Y, which is in turn fixed by Glu45 and Gln262. Water Y is visible in several SHC structures and connected via a chain of four water molecules to the cytosol. Therefore, the proton accepted by X (or left behind at Y) is easily transferred to the cytosol, completing the reaction.

Several steps of the cation cascade are obviously favored by the respective local environment. After protonating squalene, Asp376 is most likely stabilized by a positively charged His451 that in turn is electrostatically stabilized by the solvent-accessible and therefore negatively charged Glu454. The first two carbocations at C2 and C6 are electrostatically stabilized by a negative charge at Asp374-Oδ1 at a distance of 4.7 Å and by the π-electrons and dipoles of Trp312, Phe365, Tyr420, Trp489, Tyr495, Tyr609, and Tyr612 at distances from 3.5 Å to 5.5 Å. A negative charge at 374-Oδ1 is most likely because this atom is stabilized by hydrogen bonds to two amides similar to the oxanion in serine proteases, and also because 374-Oδ2 forms a strong hydrogen bond to Oδ2 of Asp377, the Oδ1 atom of which has no polar partners. The third carbocation at C10 is already at an 8 Å distance to the charge at 374-Oδ1 but close to the stabilizing dipole of Tyr420. A putative fourth cation at C15 after the formation of the 6-6-5 tricycle must be short lived because it has no stabilizing partner. In contrast, the fifth cation at C19 generated with the 6-6-6-5 tetracycle is well accommodated, interacting with the π-electrons of Phe601, Phe605, and Trp169, as supported by mutagenesis studies on these residues [23]. This provides time for the last double bond to reach the C19 cation in a complicated movement. The sixth and final hopenyl cation at C23 emerging after ring E closure is stabilized by the Phe605 π-electrons.

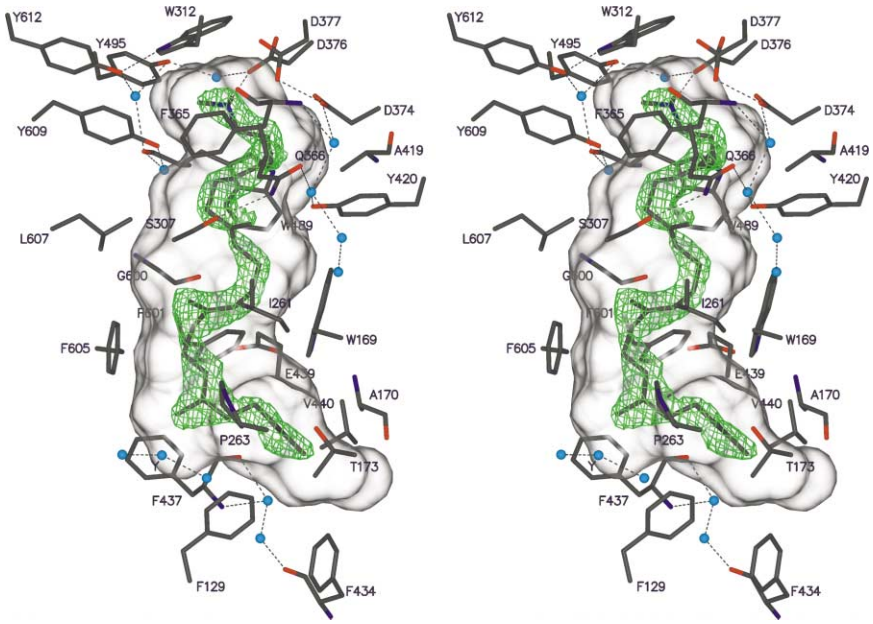

Figure 2. Stereoview of the Bound Inhibitor 2-Azasqualene in Subunit B of the Crystal Structure Showing a Well-Defined Meandering Conformation

All residues and water molecules within a distance of 4.5 Å are depicted. The (F_o-F_c)-electron density map after the initial rigid body refinement is shown at a contour level of 3 σ. The molecular envelope of the active center cavity is drawn at 1.4 Å radius [33]. The orientation of the squalene analog corresponds to Figure 1A after rotating clockwise by 90°.

Each of the molecular dynamics runs using 6-, 6-6-, 6-6-5-, 6-6-6-5-, and 6-6-6-6-5-cations converged within 0.3 Å to a specific position despite quite different starting positions (rmsd about 1.2 Å). Conspicuously, the C10′ methyl of all models remained in a bulge of the cavity at Ile261, indicating that during cyclization squalene contracts from both ends toward its center at C10′. Accordingly, the distances of the C2 and C23 atoms of the 6-6-6-6-5 pentacycle to the proton donating Asp376 and to the proton accepting water molecule Y become 4.3 Å and 6.2 Å, respectively. This leaves enough space for the putative deprotonating water X in between the pentacycle and water Y (Figure 3B).

Concerted reactions in the cyclization cascade have been under lively discussion [24]. The observed squalene binding structure permits all cyclizations up to the 6-6-6-5 tetracycle cation to occur with merely small displacements and thus almost concomitantly. At this point, however, the complicated movement of the last isoprene unit needs time, defining a long-lived intermediate. It should be noted that the biosynthetic pathway to steroids avoided this difficulty by dispensing with ring E. Moreover, the 6-6-6-5 tetracycle cation of the homologous lanosterol synthetases is only weakly stabilized, as these possess only Phe601, whereas Trp169 and Phe605 are exchanged for His and Cys, respectively, as derived from an alignment of 13 SHC and 9 lanosterol synthetase sequences (data not shown).

Before and after the reaction, squalene and hopene have to pass through the nonpolar channel (Figure 1B) connecting the active center cavity to the membrane interior. In the crystal structures, this channel is clearly too narrow for hopene. Now, the reported high-resolution structure revealed that the wall between channel and dimer surface is rather mobile, as documented in the chain mobility plot of Figure 1B. Consequently, the channel cross-section can be appreciably enlarged by melting and displacing the mobile peptide. Such an opening is particularly likely since the cyclization cascade produces an energy of about 200 kJ/mol that has to be dissipated, explaining why the bulky hopene can be released into the membrane.

Significance

The cyclization of the triterpene squalene has captivated chemists for half a century [8–10]. The enzymatic reaction was considered particularly complex, yielding the multicyclic compounds hopene in bacteria, lanosterol in vertebrates and fungi, and cycloartenol in plants. The regio- and stereoselectivity during catalysis is remarkable as, for instance, with hopene, nine stereocenters are created in one reaction sequence (Figure 1A). The bacterial pentacyclic hopene is the precursor of a wide variety of hopanoids that play a vital role in stabilizing the membranes. The eukaryotic tetracyclic lanosterol gives rise to the large group of steroids acting as hormones and as membrane components. The reported high-resolution structure of an enzyme complex with a close analog of squalene shows the exact geometry of the cyclizations and thus provides a solid experimental foundation for further theoretical analyses of the reaction [19–21]. Moreover, the deduced pathway reveals a long-lived reaction intermediate occurring before the formation of the fifth

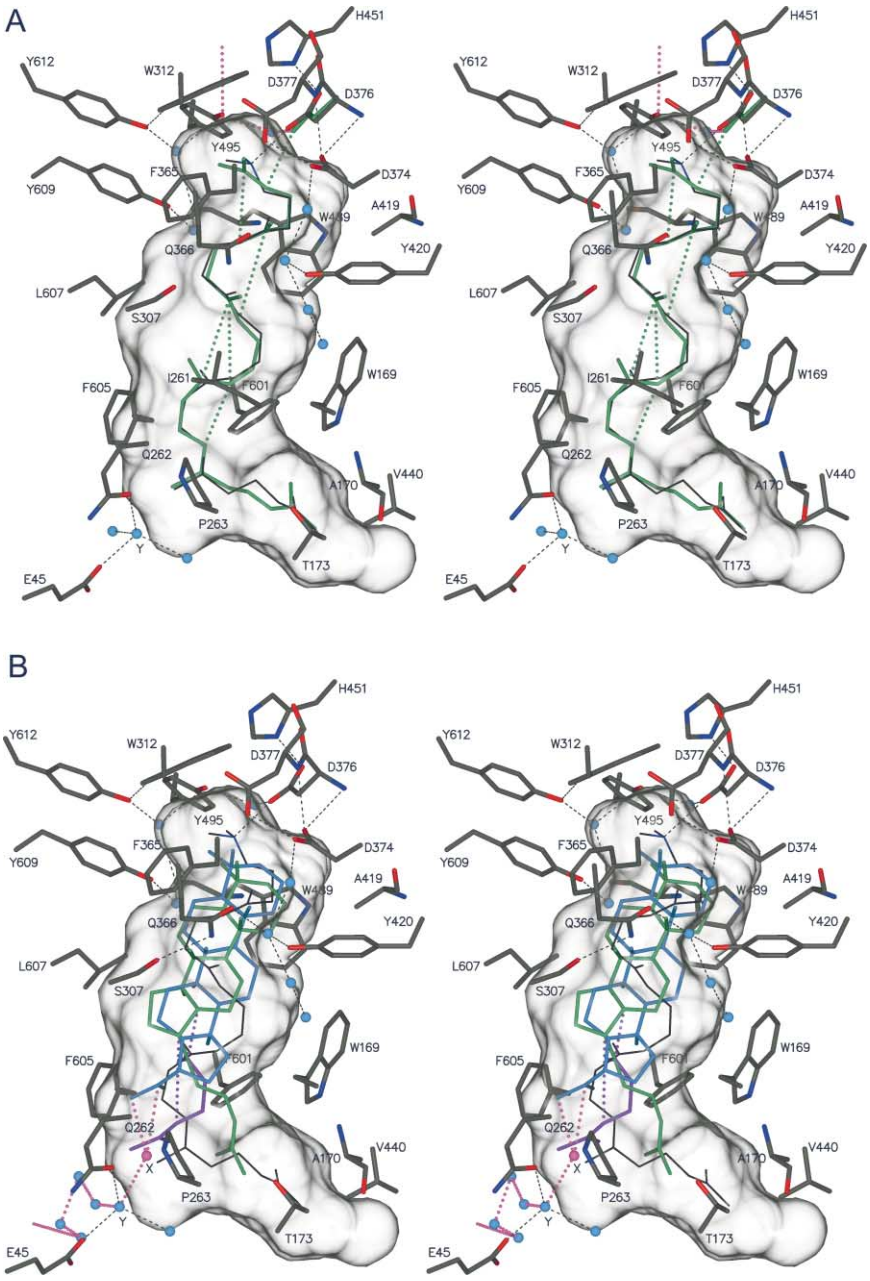

Figure 3. Stereoview of the Cyclization Reaction

All models are derived from molecular dynamics runs [27]. The observed 2-azasqualene structure (thin dark lines) is given for reference.

(A) Squalene model (green) indicating the first four carbocation additions to double bonds (green dots) that run through cations at C2, C6, C10, C14-C15, and C19 to yield the 6-6-6-5 tetracycle. The second copy of the protonating Asp376 (green) is from an inhibitor-free structure (see main text). Asp376 is reprotonated from the cytosol (pink dots).

(B) Models of the tetracycle (green) and the hopenyl cation (blue). Ile261 is omitted for clarity. For a concomitant D ring expansion and E ring formation, the 22-23 double bond has to move (green to purple). The deprotonation path (pink dots) from C23′ via water X (pink) to the cytosol is indicated. Occasionally, water X adds to C23 as a hydroxyl group.

ring. This intermediate is circumvented in the eukaryotic enzymes.

Experimental Procedures

The SHC from *A. acidocaldarius* was overexpressed in *E. coli* and the cell debris was isolated. The cytoplasmic membranes were selectively solubilized, and a heat denaturation step removed most of the host proteins. Further purification by ion exchange and size exclusion chromatography was performed as described [25]. As previously reported [15], SHC was dialyzed overnight against 0.6% (w/v) octyltetraoxyethylene (C_8E_4) in degassed bidestilled water saturated with nitrogen gas, incubated for 15 min at 55°C with a 1.5-fold molar excess of 2-azasqualene, and then crystallized by hanging-drop vapor diffusion at 20°C using equal-sized drops of a 13 mg/ml protein-inhibitor solution and of the reservoir (100 mM sodium citrate [pH 4.8], 100 mM NaCl, 6%–16% (v/v) polyethyleneglycol-600). The crystals grew within two weeks to sizes of 1500×1500×300 μm^3. They were transferred to storage buffer (1.5 M ammonium

Table 1. Data Collection and Refinement

Resolution range [Å]	20–2.13 (2.19–2.13)
Unique reflections	149,921 (11,956)
Multiplicity	5.5 (4.5)
R_{sym-I} (%)	5.2 (28.5)
Completeness (%)	99.4 (99.9)
I/σ_I	18.2 (4.9)
R_{cryst}/R_{free} (test set 2.5%)	0.186/0.228
Average B factors [Å^2]	
TLS-corrected protein chain A/B/C	25/25/25
2-azasqualene in chain A/B/C	40/31/32

The space group was $P3_221$ with unit cell axes a = b = 139.1 Å, c = 240.7 Å, and the three subunits A, B, and C in the asymmetric unit. The data were collected at a wavelength of 0.98005 Å at beamline X06SA of the Swiss Light Source (Villigen/CH). The values for the highest resolution shell are in parentheses. The resulting rmsd bond lengths and bond angles were 0.013 Å and 1.3°, respectively. The average B factor derived from a Wilson plot was 39 Å^2.

phosphate, 100 mM sodium citrate [pH 4.8], 100 mM NaCl, 0.3% (w/v) C_8E_4, 10% (w/v) glycerol), cryo-protected by increasing the glycerol content to 25% in three steps within 8 min, and then flash frozen to 100 K.

The data were collected from a single crystal at 100 K and processed with XDS [26]. A water- and ligand-free SHC [15] was used as the initial model. After rigid-body refinement with CNS [27], a difference-Fourier map outlined 2-azasqualene in detail. The models of 2-azasqualene, squalene, and its derivatives were generated with SYBYL (Tripos, St. Louis), and the topology and parameter files were generated with PRODRG [28]. All model manipulations were done with program O [29]. Using CNS [27], the structure was refined up to an R_{cryst} (R_{free}) value of 23% (27%). Since the bulk solvent correction indicated anisotropy, the refinement was continued with REFMAC [30] using each of the three asymmetric subunits as a TLS group. All relevant data are given in Table 1. Figures were produced with POVScript+ [31] and Raster3D [32]. The molecular surface was calculated with MSMS [33].

The initial squalene model was the experimentally established 2-azasqualene with an isoprenoid carbon instead of the nitrogen. The model was adjusted by molecular dynamics using the simulated annealing, rigid body, and energy minimization routines of CNS [27] in a fixed polypeptide plus water environment. The models of the squalene derivatives were placed manually at five different collision-free positions and subjected to a molecular dynamics run as described for squalene. The resulting models were compared within each group, and the model with the smallest deviation from the four others was displayed in Figure 3.

Acknowledgments

We thank the team of the Swiss Light Source (Villingen/CH) for their help with data collection, the Deutsche Forschungsgemeinschaft for support by grant GRK-434, and the Ministero della Istruzione, Universita e Ricerca Scientifica for support by grant ex60%.

Received: October 23, 2003
Accepted: November 6, 2003
Published: January 23, 2004

References

1. Croteau, R., Kutchan, T.M., and Lewis, N.G. (2000). Natural products (secondary metabolites). In Biochemistry and Molecular Biology of Plants, B. Buchanan, W. Gruissem, and R. Jones, eds. (New York: Wiley & Sons), pp. 1250–1315.
2. Wendt, K.U., Poralla, K., and Schulz, G.E. (1997). Structure and function of squalene cyclase. Science *277*, 1811–1815.
3. Starks, C.M., Back, K., Chappel, J., and Noel, J.P. (1997). Structural basis for cyclic terpene biosynthesis by tobacco 5-epi-aristolochene synthase. Science *277*, 1815–1820.
4. Lesburg, C.A., Zhai, G., Cane, D.E., and Christianson, D.W. (1997). Crystal structure of pentalenene synthase: mechanistic insights on terpenoid cyclization reactions in biology. Science *277*, 1820–1824.
5. Caruthers, J.M., Kang, I., Rynkiewicz, M.J., Cane, D.E., and Christianson, D.W. (2000). Crystal structure determination of aristolochene synthase from the blue cheese mold, *Penicillium roqueforti*. J. Biol. Chem. *275*, 25533–25539.
6. Rynkiewicz, M.J., Cane, D.E., and Christianson, D.W. (2001). Structure of trichodiene synthase from *Fusarium sporotrichioides* provides mechanistic inferences on the terpene cyclization cascade. Proc. Natl. Acad. Sci. USA *98*, 13543–13548.
7. Whittington, D.A., Wise, M.L., Urbansky, M., Coates, R.M., Croteau, R.B., and Christianson, D.W. (2002). Bornyldiphosphate synthase: Structure and strategy for carbocation manipulation by a terpenoid cyclase. Proc. Natl. Acad. Sci. USA *99*, 15375–15380.
8. Woodward, R.B., and Bloch, K. (1953). The cyclization of squalene in cholesterol synthesis. J. Am. Chem. Soc. *75*, 2023–2024.
9. Abe, I., Rohmer, M., and Prestwich, G.D. (1993). Enzymatic cyclization of squalene and oxidosqualene to sterols and triterpenes. Chem. Rev. *90*, 2189–2206.
10. Wendt, K.U., Schulz, G.E., Corey, E.J., and Liu, D.R. (2000). Enzyme mechanisms for polycyclic triterpene formation. Angew. Chem. Int. Ed. Engl. *39*, 2812–2833.
11. Wendt, K.U., Lenhart, A., and Schulz, G.E. (1999). The structure of the membrane protein squalene-hopene cyclase at 2.0 Å resolution. J. Mol. Biol. *286*, 175–187.
12. Milla, P., Lenhart, A., Grosa, G., Viola, F., Weihofen, W.A., Schulz, G.E., and Balliano, G. (2002). Thiol-modifying inhibitors for understanding squalene cyclase function. Eur. J. Biochem. *269*, 2108–2116.
13. Feil, C., Süssmuth, R., Jung, G., and Poralla, K. (1996). Site-directed mutagenesis of putative active-site residues in squalene-hopene cyclase. Eur. J. Biochem. *242*, 51–55.
14. Ceruti, M., Balliano, G., Viola, F., Cattel, L., Gerst, N., and Schuber, F. (1987). Synthesis and biological activity of azasqualenes, bis-azasqualenes and derivatives. Eur. J. Med. Chem. *22*, 199–208.
15. Lenhart, A., Weihofen, W.A., Pleschke, A.E.W., and Schulz, G.E. (2002). Crystal structure of a squalene cyclase in complex with the potential anticholesteremic drug Ro48–8071. Chem. Biol. *10*, 639–645.
16. Burley, S.K., and Petsko, G.A. (1985). Aromatic-aromatic interaction: A mechanism of protein structure stabilization. Science *229*, 23–28.
17. Brandl, M., Weiss, M.S., Jabs, A., Sühnel, J., and Hilgenfeld, R. (2001). CH···π-interactions in proteins. J. Mol. Biol. *307*, 357–377.
18. Lenhart, A., Reinert, D.J., Aebi, J.D., Dehmlow, H., Morand, O.H., and Schulz, G.E. (2003). Binding structures and potencies of oxidosqualene cyclase inhibitors with the homologous squalene-hopene cyclase. J. Med. Chem. *46*, 2083–2092.
19. Jenson, C., and Jorgensen, W.L. (1997). Computational investigations of carbenium ion reactions relevant to sterol biosynthesis. J. Am. Chem. Soc. *119*, 10846–10854.
20. Hess, B.A., Jr. (2003). Formation of the C ring in the lanosterol biosynthesis from squalene. Org. Lett. *5*, 165–167.
21. Hess, B.A., Jr. (2002). Concomitant C-ring expansion and D-ring formation in lanosterol biosynthesis from squalene without violation of Markovnikov's rule. J. Am. Chem. Soc. *124*, 10286–10287.
22. Pale-Grosdemange, C., Feil, C., Rohmer, M., and Poralla, K. (1998). Occurrence of cationic intermediates and deficient control during the enzymatic cyclization of squalene into hopenoids. Angew. Chem. Int. Ed. Engl. *37*, 2237–2240.
23. Hoshino, T., and Sato, T. (2002). Squalene-hopene cyclase: catalytic mechanism and substrate recognition. Chem. Commun. (Camb.), 291–301.
24. Corey, E.J., Virgil, S.C., Cheng, H., Baker, C.H., Matsuda, S.P.T., Singh, V., and Sarshar, S. (1995). New insights regarding the cyclization pathway for sterol biosynthesis from (S)-2,3-oxidosqualene. J. Am. Chem. Soc. *117*, 11819–11820.
25. Wendt, K.U., Feil, C., Lenhart, A., Poralla, K., and Schulz, G.E. (1997). Crystallization and preliminary X-ray crystallographic

analysis of squalene-hopene cyclase from *Alicyclobacillus acidocaldarius*. Protein Sci. *6*, 722–724.
26. Kabsch, W. (1993). Automatic processing of rotation diffraction data from crystals of initially unknown symmetry and cell constants. J. Appl. Crystallogr. *26*, 795–800.
27. Brünger, A.T., Adams, P.D., Clore, G.M., DeLano, W.L., Gros, P., Grosse-Kunstleve, R.W., Jiang, J.-S., Kuszewski, J., Nilges, M., Pannu, N.S., et al. (1998). Crystallography & NMR system: a new software for macromolecular structure determination. Acta Crystallogr. D Biol. Crystallogr. *54*, 905–921.
28. van Aalten, D.M.F., Bywater, R., Findlay, J.B.C., Hendlich, M., Hooft, R.W.W., and Vriend, G. (1996). PRODRG, a program for generating molecular topologies and unique molecular descriptors from coordinates of small molecules. J. Comput Aided Mol. Des. *10*, 255–262.
29. Jones, T.A., Zou, J.-Y., Cowan, S.W., and Kjeldgaard, M. (1991). Improved methods for building protein models in electron density maps and the location of errors in these models. Acta Crystallogr. A *47*, 110–119.
30. Murshudov, G.N., Vagin, A.A., and Dodson, E.J. (1997). Refinement of macromolecular structures by the maximum-likelihood method. Acta Crystallogr. D Biol. Crystallogr. *53*, 240–255.
31. Fenn, T.D., Ringe, D., and Petsko, G.A. (2003). POVScript+: a program for model and data visualization using persistence of vision ray-tracing. J. Appl. Crystallogr. *36*, 944–947.
32. Merritt, E.A., and Bacon, D.J. (1997). RASTER 3D: Photorealistic molecular graphics. Methods Enzymol. *277*, 505–524.
33. Sanner, M.F., Olson, A.J., and Spehner, J.-C. (1996). Reduced surface: An efficient way to compute molecular surfaces. Biopolymers *38*, 305–320.